

---

## A first assessment of organic carbon burial in the West Gironde Mud Patch (Bay of Biscay)

Dubosq Nicolas <sup>1,\*</sup>, Schmidt Sabine <sup>2</sup>, Walsh J.P. <sup>3</sup>, Grémare Antoine <sup>1</sup>, Gillet Hervé <sup>1</sup>, Lebleu Pascal <sup>1</sup>, Poirier Dominique <sup>1</sup>, Perello Marie-Claire <sup>1</sup>, Lamarque Bastien <sup>1</sup>, Deflandre Bruno <sup>1</sup>

<sup>1</sup> Univ. Bordeaux, CNRS, EPOC, EPHE, UMR 5805, F-33615, Pessac, France

<sup>2</sup> CNRS, Univ. Bordeaux, EPOC, EPHE, UMR 5805, F-33615, Pessac, France

<sup>3</sup> Coastal Resources Center, University of Rhode Island, Kingstown, RI 02881, USA

\* Corresponding author : Nicolas Dubosq, email address : [nicolas.dubosq@u-bordeaux.fr](mailto:nicolas.dubosq@u-bordeaux.fr)

---

### Abstract :

On the Bay of Biscay continental shelf, there are several mid-shelf mud patches including La Grande Vasière to the north, the West Gironde Mud Patch (WGMP) off the Gironde estuary and the Basque Mud Patch close to the Spanish border. In general, these deposits are several meters thick and cover coarser substrate. Questions remain about their storage capability for fine particles and carbon. This work investigates the sedimentation of the WGMP in order to develop a first estimate of organic carbon (OC) burial. Interface sediment cores were collected at nine stations along two cross-shelf transects in October–November 2016. X-radiograph imaging and grain-size analyses were used to characterize sedimentary structures. 210Pbxs depth profiles were established to calculate sediment (SAR) and mass (MAR) accumulation rates. Sedimentary structures indicate episodic sandy inputs overlying older deposits at proximal sites, and relatively continuous sedimentation at seaward locations. On the outer-central portion of the northern transect, a maximum SAR (0.47 cm yr<sup>-1</sup>) was observed, suggesting a depocenter. On the southern transect, excluding two stations where sedimentary inputs appear massive but sporadic, the SARs are lower (<0.3 cm yr<sup>-1</sup>). Quantitative estimates of OC burial rates increase seaward with a maximum of 45 gC m<sup>-2</sup> yr<sup>-1</sup>. To evaluate carbon loading independent of grain-size variability, OC values were normalized to surface area of sediments (SA). Interestingly, a qualitative comparison of OC burial efficiencies using the OC/SA ratio highlights three groups of sites (low, medium and relatively high OC burial efficiency) which are likely related both to different sedimentary environments and variable deposition conditions linked to local environmental conditions and depth. This work highlights the likely control of hydrodynamic intensity and sedimentary inputs on the amount of OC stored in the WGMP sediments.

### Highlights

► The West Gironde Mud Patch can be divided in three deposition areas ► Organic carbon (OC) burial rates increase seaward with a maximum of 45 gC m<sup>-2</sup> yr<sup>-1</sup> ► Hydrodynamic seems to control organic carbon burial at a multi-decennial scale ► OC burial rates and efficiencies vary depending on bathymetry

---

**Keywords** : sediment accumulation rate, organic carbon burial, West Gironde Mud Patch, Bay of Biscay, continental shelf

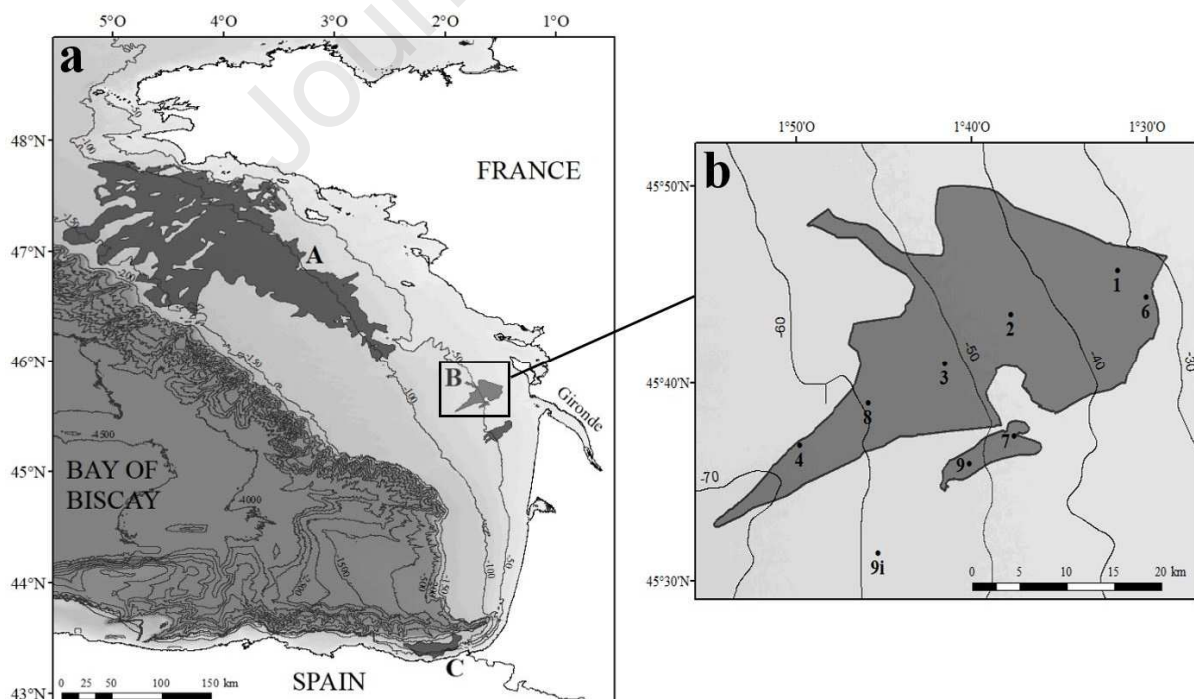
## 35 **1. Introduction**

36 Organic carbon storage in marine sediments is recognized as a long-term sink for atmospheric  
37 carbon dioxide (Bernier, 1990, 1982). Understanding the ocean carbon cycle and quantifying  
38 carbon storage in the oceans are therefore crucial for improving future climate scenarios  
39 (Blair and Aller, 2012; Burdige, 2007; Keil, 2017; Muller-Karger, 2005; Włodarska-  
40 Kowalczyk et al., 2019). With about 90% of the modern organic carbon preservation  
41 occurring in Rivers-dominated Ocean Margins (RiOMars) systems (Hedges and Keil, 1995;  
42 McKee et al., 2004), special attention should be paid to these areas. Although three types of  
43 RiOMars have been defined by Blair and Aller (2012), it can be difficult to understand the  
44 nature of an individual system because of high spatial and temporal variability (McKee et al.,  
45 2004). Owing to these variabilities, each RiOMar can be divided in several sub-environments  
46 where major organic carbon (OC) preservation controlling factors may be different (McKee et  
47 al., 2004). Moreover, most studies of RiOMars have focused on tropical systems whose  
48 results are difficult to translate to higher latitudes (Yao et al., 2014; Zhu et al., 2016). This  
49 explains why, in spite of numerous studies on RiOMars (e.g. Aller, 1998; Aller et al., 1996,  
50 1986; Aller and Blair, 2006; Blair and Aller, 2012; Deng et al., 2006; Kuzyk et al., 2017;  
51 McKee et al., 2004; Pastor et al., 2018, 2011; Yao et al., 2014; Zhu et al., 2013 and references  
52 therein), mechanisms controlling OC preservation in these environments as well as their  
53 carbon burial capabilities are not yet fully understood and quantified.

54 On the Northeast Atlantic margin, the Bay of Biscay continental shelf extends over more than  
55 1000 km, from the Celtic to the North Iberian margins (Borja et al., 2019; Bourillet et al.,  
56 2006; Schmidt et al., 2014). Surface shelf sediments are mainly sand. However on the shelf lie  
57 also several mid-shelf mud belts and patches including (1) “La Grande Vasière” to the north,  
58 (2) the West Gironde Mud Patch off the Gironde estuary and (3) the Basque Mud Patch in  
59 front of San Sebastian and Bayonne (**Figure 1**, Allen and Castaing, 1977; Jouanneau et al.,  
60 2008, 1999; Lesueur et al., 2002). Overall they are of several meters thick and cover coarser  
61 substrate (Jouanneau et al., 1999, 1989; Lesueur et al., 2002, 2001). Mud belts and patches are  
62 found on many continental shelves around the world. Typically, they are bounded by dynamic  
63 sands on their landward side and are the result of river-derived sediment deposition in areas of

64 lower hydrodynamics (i.e., where waves and currents are more reduced on the seabed;  
 65 McCave, 1972; Walsh and Nittrouer, 2009). Indeed, their mid-shelf location is directly related  
 66 to the fact that higher-energy conditions at shallower depth closer to the coast preclude fine  
 67 sediment accumulation (Dias et al., 2002; McCave, 1972; Walsh and Nittrouer, 2009). These  
 68 areas are important for biogeochemical transformations and are known organic carbon sinks  
 69 (McKee et al., 2004).

70 The West Gironde Mud Patch is particularly interesting because it is under the influence of  
 71 the Gironde estuary which is the major source of fine sediments for the Bay of Biscay  
 72 continental shelf (Constantin et al., 2018; Jouanneau et al., 1999, 1989; Lesueur et al., 2002,  
 73 1996, 1991; Weber et al., 1991). Studies led in 1990's have rather well defined its  
 74 sedimentary functioning and suggested a control of sedimentation and resuspension processes  
 75 by hydrodynamics (Jouanneau et al., 1989; Lesueur et al., 2002, 1991). Only few studies have  
 76 focused on the WGMP biogeochemistry and ecology (i.e., Massé et al., 2016; Relexans et al.,  
 77 1992), and have performed too few measurements to characterize its sedimentological,  
 78 biogeochemical and ecological functioning. This explains why the capability of the WGMP to  
 79 store OC has not yet been estimated. The present study aims therefore to characterize  
 80 sedimentation intensity and preferential areas of sediment accumulation in the WGMP to  
 81 conduct a first estimate of OC burial rates and efficiencies along two cross-shelf bathymetric  
 82 transects.



83  
 84 **Figure 1:** (a) Map of the Bay of Biscay continental shelf with the locations of mud belts and patches: A - La Grande Vasière,  
 85 B - The Gironde Mud Patches, and C - The Basque Mud Patch. (b) Map of the WGMP showing the location of sampling

86 stations (black circles). The synoptic map of the West Gironde Mud Patch has been determined during the JERICOBENT-5-  
87 TH cruise (Gillet and Deflandre, 2018)

## 88 2. Material and methods

### 89 2.1 Study site

90 Formed during the Holocene by filling a depression interpreted as a paleo-valley (Lesueur et  
91 al., 2002, 1996), the West Gironde Mud Patch is a silty clay sedimentary patch located in the  
92 Bay of Biscay, about 15 km seaward of the Gironde estuary mouth (Jouanneau et al., 1989). It  
93 lies between 30 and 75 m depth with a surface of about 420 km<sup>2</sup> (Jouanneau et al., 1989;  
94 Lesueur et al., 1991; Massé et al., 2016). The WGMP is influenced by Gironde inputs  
95 (Constantin et al., 2018; Jouanneau et al., 1989; Lesueur et al., 2002), which are the highest  
96 during river floods (Constantin et al., 2018; Lesueur et al., 2002). On a historical scale,  
97 climatic fluctuations (e.g. the “Little Ice Age”) and anthropogenic activities like deforestation  
98 during the medieval period or estuary management since the XIX<sup>th</sup> century (e.g. dredging,  
99 channel hardening) seem to have modified sediment transport processes and therefore the  
100 amount of sediments exported to the shelf (Lesueur et al., 2002, 1996). Sediments are  
101 transported from the estuary to the WGMP in a benthic nepheloid layer and believed to be  
102 deposited in its deeper part (Weber et al., 1991). During their sedimentation, estuarine  
103 particles are mixed with biogenic material (e.g. diatoms) produced in the water column  
104 (Weber et al., 1991). In the proximal WGMP, sandy inputs from the adjacent continental shelf  
105 can be mixed with silt and clay sediments during storm events (Lesueur et al., 2002; Weber et  
106 al., 1991).

### 107 2.2 Sampling

108 The JERICOBENT-1 cruise took place in October - November 2016 on the R/V *Côtes de la*  
109 *Manche* (Deflandre, 2016). Undisturbed sediment cores were collected using a MC6 *Octopus*  
110 *GmbH* multicorer on two transects (**Figure 1**). The northern transect includes five stations (1,  
111 2, 3, 8 and 4), and the southern one has four stations (6, 7, 9 and 9i). At each site, three cores  
112 were used to characterize sedimentation. A sediment core (core A) was carefully extruded for  
113 radioisotope measurements, every 0.5 cm from the top core to 4 cm and every 1 cm below  
114 until the core bottom. A second core (core B) was sliced for organic carbon content and  
115 sediment surface area measurements every 0.5 cm over the first centimeter, every 1 cm until 5  
116 cm then every 2 cm until 21 cm and every 5 cm below. All the samples were immediately  
117 frozen aboard the ship and kept in the freezer until analysis. An additional sediment core was

118 preserved for X-ray imaging (core C), which was performed within a few days after sampling.  
119 Due to the thinness of the mud, station 9i was only sampled for radioisotope measurements  
120 before repositioning the vessel.

## 121 2.2 Physical characteristics of sediments

122 Radiographical images which provide a continuous record of sedimentary structures were  
123 performed on a longitudinal section of the preserved sediment core using an X-ray imaging  
124 system (SCOPIX). Images recorded were converted in 8 bits to bring out sedimentary  
125 structures at high resolution (Lofi and Werber, 2001). Dry bulk density (DBD) was calculated  
126 on core A by comparing sediment weight before and after drying at 60°C according to the  
127 following expression:  $DBD = (1 - (V_w / (V_w + V_s))) * \rho$  with  $V_w$  and  $V_s$  respectively volumes of  
128 water and particles in the sample and  $\rho$ , particle density (i.e., 2.65 g cm<sup>-3</sup>). Sediment grain-  
129 size was measured on cores A and B using a Malvern Mastersizer 2000 laser diffraction  
130 particle size analyzer. The grain-size distributions being unimodal with the exception of three  
131 samples within sandy layers (i.e. cores B, St. 1: 0.5-1 cm, 1-1.5 cm; St. 4: 20-22 cm), median  
132 grain-size (D50) and sand content were used as grain-size descriptors.

## 133 2.3 Radionuclide analysis

134 The sedimentation framework was determined based on <sup>210</sup>Pb. <sup>210</sup>Pb ( $T_{1/2} = 22.3$  years) is a  
135 naturally-occurring radionuclide continuously delivered by atmospheric fallout and *in situ*  
136 production. This <sup>210</sup>Pb, readily scavenged by the particulate phase in the water column and  
137 deposited at the seabed by sedimentation, is referred to as <sup>210</sup>Pb in excess (<sup>210</sup>Pb<sub>xs</sub>) of that  
138 found within sediment due to the decay of its parent isotope, <sup>226</sup>Ra. Radionuclide activities  
139 (<sup>210</sup>Pb, <sup>226</sup>Ra) were measured using a high-efficiency, broad energy gamma detector equipped  
140 with a Cryo-Cycle II (Mirion). The  $\gamma$  detector is calibrated using IAEA certified materials  
141 (RGU-1). Errors on activities are based on standard deviation counting statistics. Excess <sup>210</sup>Pb  
142 activities were calculated by subtracting the activity supported by its parent, <sup>226</sup>Ra, from the  
143 total <sup>210</sup>Pb activity in the sediment. Sediment layers were measured downcore until reaching  
144 negligible <sup>210</sup>Pb<sub>xs</sub> activities or the bottom of the core. Sediment and mass accumulation rates  
145 (SAR and MAR, respectively) were calculated below the mixed layers from the slope of the  
146 <sup>210</sup>Pb<sub>xs</sub> profiles against depth and cumulative mass, respectively, using the CF:CS (constant  
147 flux and constant sedimentation) model.

148 It must be noted that <sup>137</sup>Cs could be also detected during the same counting sessions. The  
149 occurrence of <sup>137</sup>Cs ( $T_{1/2} = 30$  years), an artificial radionuclide, is primarily the result of the

150 nuclear weapon test fallout in the early 1960s. In coastal sediments, its detection is an  
151 indicator of sediment deposited since 1950.  $^{137}\text{Cs}$  activities present low to negligible activities  
152 in WGMP sediments, and are not presented in this work. Data (radionuclides, grain-size, dry  
153 bulk density) are openly available in a public repository that issues datasets with DOIs  
154 (Schmidt, 2020).

#### 155 *2.4 Particulate organic carbon*

156 OC content was measured on freeze-dried pre-weighed sediments using a LECO CS 200. In  
157 order to remove carbonates before analysis, an aliquot of about 100 mg was acidified with  
158 HCl 2M and dried at 50°C (Cauwet et al., 1990; Etcheber et al., 1999). Sample was then  
159 introduced into a furnace where particulate OC combustion produced carbon dioxide which  
160 was quantitatively dosed by infrared absorption (Etcheber et al., 1999). The reproducibility of  
161 replicated analyses was better than 5%.

162 Organic carbon contents were normalized to surface area of sediments (SA, expressed in  $\text{m}^2 \text{g}^{-1}$ )  
163 to minimize variations due strictly to grain-size changes (Hedges and Keil, 1995; Mayer,  
164 1994a). A subsample of freeze-dried sediments was first homogenized and degassed  
165 overnight at 150°C. SA was then assessed using a Gemini® VII Surface Area Analyzer  
166 (2390a model; Micromeritics®) by a multi-point BET method (Aller and Blair, 2006; Mayer,  
167 1994a).

#### 168 *2.5 Statistical treatment*

169 The significance of correlations between median grain-size and surface area of the sediments  
170 and between surface area and organic carbon content was assessed using a Spearman's rank  
171 correlation coefficient. These analyses were run with the software SigmaPlot version 14.

### 172 **3. Results**

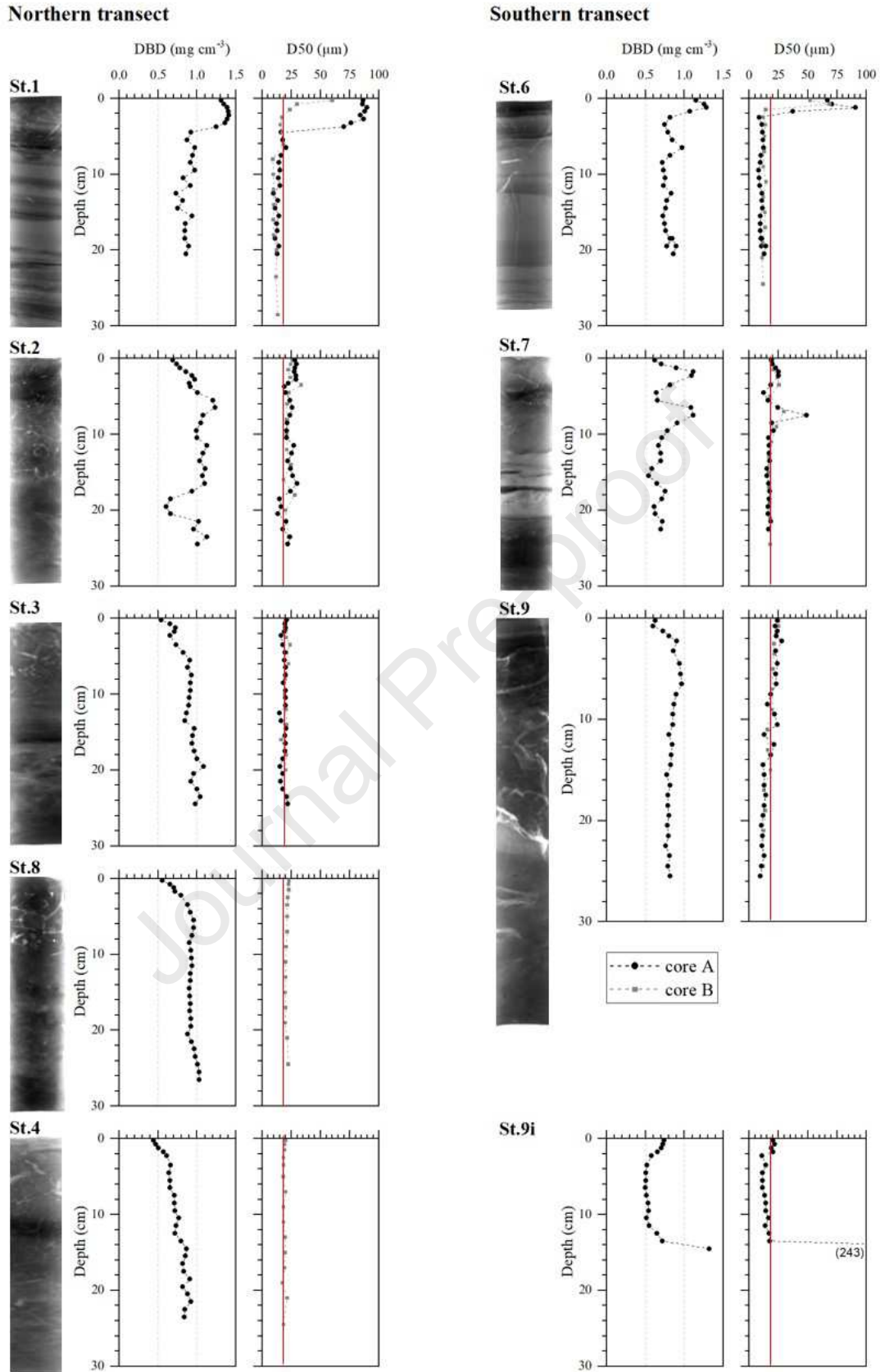
#### 173 *3.1 Physical characteristics of sediments and sedimentary structures*

174 Sedimentary environments vary in the WGMP. Indeed, although sediments are mainly silt and  
175 clay with a median grain-size of 15-20  $\mu\text{m}$ , some peripheral stations (i.e., 1, 6 and 7) have  
176 deposits of varying silty and sandy sediments (**Figure 2**). At these sites, median grain-size is  
177 higher than 20  $\mu\text{m}$  in some layers of higher sand content (>6%, **Figure 2**). Moreover, the base  
178 of these layers is characterized by an erosive contact. The two most proximal stations (i.e., 1  
179 and 6) stand out by having a sandy layer on core top. Based on the grain-size profiles and X-  
180 ray images, the thickness of this layer varies from 1 to 4 cm at station 1 depending on cores,

181 which indicates a high spatial variability in the proximal area. Below this surface layer,  
182 median grain-size is rather constant with depth but finer than the size measured at other sites,  
183 with values around 12 and 10  $\mu\text{m}$  at stations 1 and 6, respectively. Interestingly, similar finer  
184 sediments are observed at station 9 from a depth of 17 cm. X-ray images also highlight the  
185 presence of thin sandy layers at the shallowest stations (i.e., 1, 2, 3, 6, and 7) which become  
186 less frequent with increasing depth (**Figure 2**).

187 The dry bulk density increases in depth on cores with a rather constant grain-size (e.g. stations  
188 8 and 4, **Figure 2**) as usually observed in interface sediments because of sediment  
189 compaction. On the contrary, DBD profiles show variations, usually related to sandy layers,  
190 on cores 1, 2, 6, 7 and 9i. These laminae are well preserved in the proximal area (i.e., stations  
191 1 and 6) and at station 7 compared to more distal sites (i.e., 8 and 4) where sediments are  
192 homogeneous. The station 9i, at the end of the southern transect is different from the other; it  
193 is characterized by a mud deposit of about 14 cm covering a medium sand substratum (**Figure**  
194 **2**).



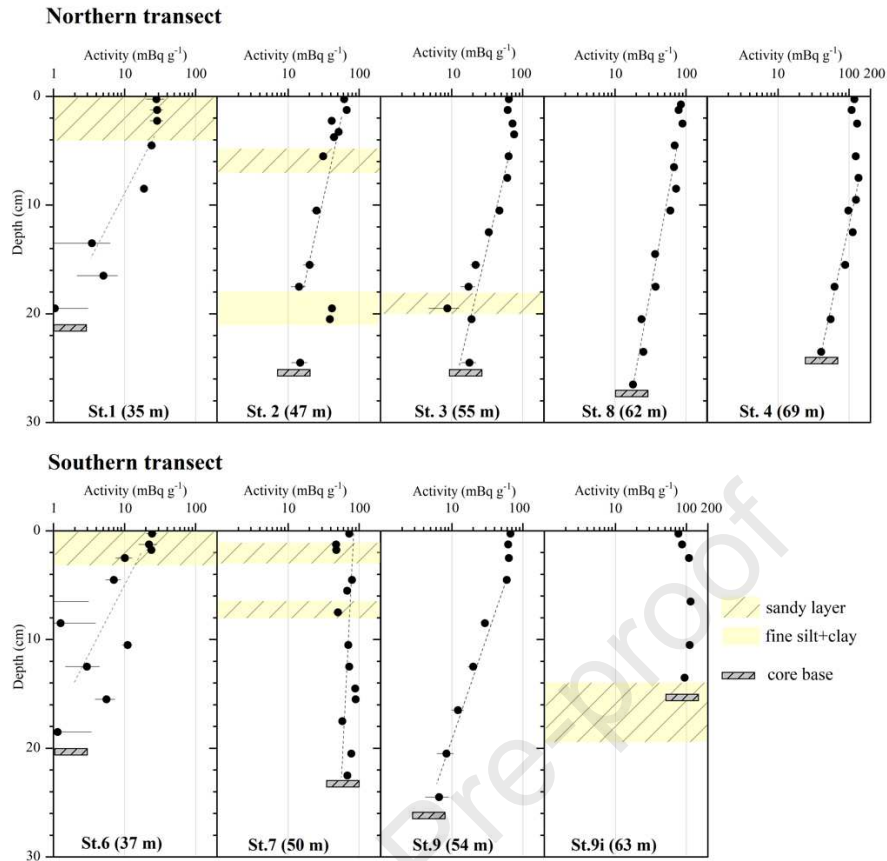


195

196 **Figure 2:** Sedimentary structures: X-ray images and profiles of dry bulk density and median grain-size with depth of cores  
 197 collecting along the northern (left) and southern (right) transects. The red line defines the background grain-size ( $\sim 20 \mu\text{m}$ ),  
 198 and in some cases higher sand content is observed ( $>6\%$ ).

199 3.2  $^{210}\text{Pb}$  profiles in interface sediments

200 Along the two depth transects, surface excess  $^{210}\text{Pb}$  ranged between 24 and 111  $\text{mBq}^{-1}$ ,  
201 increasing with depth (**Figure 3**). However, the small difference of depth among sites  
202 (affecting water column production) cannot account for such low activities at sites 1 and 6.  
203 Rather, the lower activities are likely due to dilution by sand. There are three types of  $^{210}\text{Pb}_{\text{xs}}$   
204 profiles. The first group corresponds to the proximal stations 1 and 6. The two most proximal  
205 stations present low surface activities, associated with sand, and a rapid activities decrease  
206 with depth to reach almost supported levels at about 10-15 cm. These profiles reflect rather  
207 low mean apparent sediment and mass accumulation rates, about  $0.1\text{-}0.2 \text{ cm yr}^{-1}$  and  $< 200$   
208  $\text{mg cm}^{-2} \text{ yr}^{-1}$  (**Table 1**). The second group includes stations 7 and 9i along the southern  
209 transect, and to a less extent station 2 in the north. The cores present evidence of  
210 heterogeneities with depth, as revealed by X-ray images, grain-size and dry bulk density  
211 (**Figure 2**, see section 3.1). Such changes in the sediment are likely to impact the  $^{210}\text{Pb}_{\text{xs}}$   
212 activities and are not related to decay. These deep penetration of  $^{210}\text{Pb}_{\text{xs}}$  with depth in the  
213 sediment associated with a low activity decrease could reflect massive deposition events. The  
214 last group corresponds to cores of the WGMP outer and deepest area, on the north stations 3,  
215 8, and 4 and on the south station 9. At these stations,  $^{210}\text{Pb}_{\text{xs}}$  profiles present a surface mixed  
216 layer, followed by a penetration at depths deeper to 25-30 cm. The mixed layer is comprised  
217 from 3-4 cm at stations 3 and 8 to 8-9 cm at station 4, indicating an increase of its thickness  
218 with depth. Sediment and mass accumulation rates range between  $0.29$  to  $0.47 \text{ cm yr}^{-1}$  and  
219  $237$  to  $438 \text{ mg cm}^{-2} \text{ yr}^{-1}$ . Along the northern transect, the highest SARs and MARs are  
220 observed at mid-depths (around 50 m). These results are consistent with the outcome of a first  
221 investigation of the WGMP sedimentation, based on less vertically-detailed  $^{210}\text{Pb}_{\text{xs}}$  profiles  
222 established on cores sampled in 1995 (Lesueur et al., 2001).



223

224 **Figure 3:** Depth profiles of  $^{210}\text{Pb}_{\text{xs}}$  activity for all the sediment cores collected in the West Gironde Mud Patch in fall 2016.  
 225 Next to the core label, numbers are the water depth at which the cores were collected. Errors bars correspond to 1 SD. The  
 226 grey rectangle indicates the length of the core.

227 **Table 1:** Mean bottom OC contents, sediment (SAR) and mass (MAR) accumulation rates calculated from  $^{210}\text{Pb}_{\text{xs}}$  profiles  
 228 and calculated OC burial rates at nine sites of the West Gironde Mud Patch. For stations 1, 6 and 9, the bottom OC values  
 229 were taken at the base of modern sediments (see Figure 4)

Transect	Stations	Lat.	Long.	Depth	Bottom OC	$n =$	SAR	MAR	OC burial rates
		$^{\circ}\text{N}$	$^{\circ}\text{E}$						
North	1	45°45'38"	-1°31'41"	35	0.64 ± 0.03*	1	0.14 ± 0.08**	126 ± 73**	8 ± 5**
	2	45°43'45"	-1°37'57"	47	0.66 ± 0.20	5	0.48 ± 0.09**	486 ± 89**	32 ± 16
	3	45°40'58"	-1°41'30"	55	0.99 ± 0.12	5	0.38 ± 0.04	361 ± 35	36 ± 8
	8	45°38'55"	-1°45'48"	62	1.02 ± 0.02	5	0.47 ± 0.05	438 ± 47	45 ± 6
	4	45°36'50"	-1°49'47"	69	1.30 ± 0.04	4	0.41 ± 0.07	338 ± 56	44 ± 9
South	6	45°44'22"	-1°30'2"	37	0.42 ± 0.27	2	0.22 ± 0.13**	172 ± 102**	7 ± 9**
	7	45°37'17"	-1°37'34"	50	1.41 ± 0.19	6	0.97 ± 0.20***	648 ± 122***	-
	9	45°35'54"	-1°40'9"	54	1.17 ± 0.10	3	0.29 ± 0.03	237 ± 22	28 ± 5
	9i	45°31'25"	-1°45'20"	63	-	-	2.83***	1413***	-

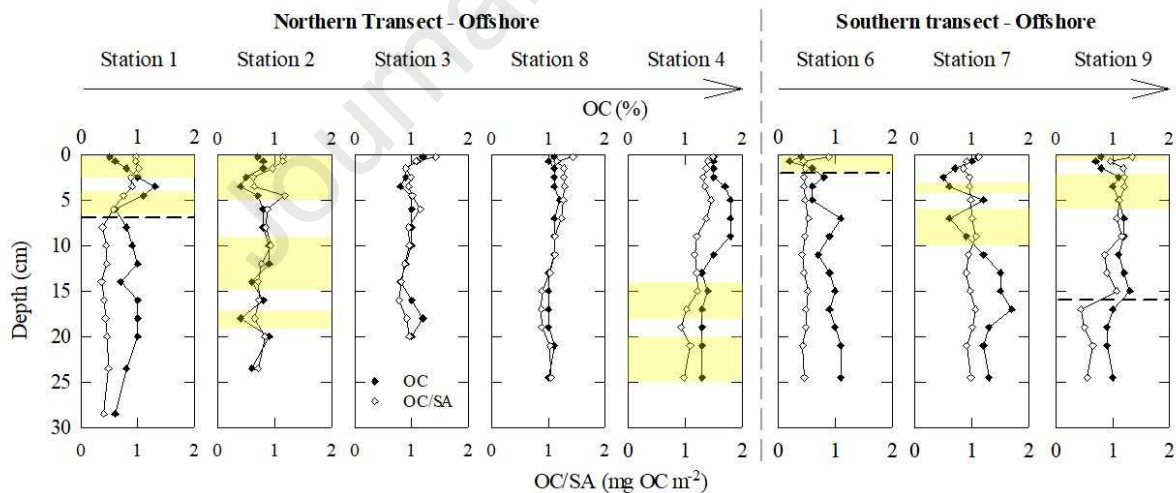
\*analytical incertitude

\*\* apparent maximum SAR, MAR and OC burial rates, presence of sandy layers

\*\*\* indicative maximum SAR and MAR - not suitable for calculations

## 230 3.3 Sedimentary organic carbon

231 Surface organic carbon contents increase seaward from 0.5 to 1.5% (**Table 2, Figure 4**) as  
 232 previously reported (Massé et al., 2016; Relexans et al., 1992). Depth OC profiles present  
 233 different patterns depending on sites as reported for  $^{210}\text{Pb}_{\text{xs}}$ . Profiles at stations 3 and 8 present  
 234 the highest values of OC at the core top which remain rather constant in the mixed layer and  
 235 then decrease in depth. This pattern is different for stations 1, 2, 6 and 7 which show more  
 236 erratic profiles where the lowest OC values appear to be associated with sandy layers (**Figure**  
 237 **4**). Mayer (1994a) demonstrated that the relation between OC content and grain-size is related  
 238 to the adsorption of organic matter on particles, and this can be reinterpreted in terms of the  
 239 surface area of sediments. Typically, larger-sized particles such as sands have a smaller  
 240 surface area than smaller-sized particles such as clays. Less organic matter is therefore  
 241 adsorbed on sandy sediments than on muddy ones. These patterns are observed for the whole  
 242 WGMP with significant correlations between grain-size and SA (p-value<0.01, **Figure 5a**)  
 243 and between SA and OC content (p-value<0.01 for the two slopes, **Figure 5c**), indicating that  
 244 the sediment OC content is at least partly controlled by the grain-size and surface area of  
 245 particles.



246

247 **Figure 4:** Vertical distributions of OC content (%) and OC/SA ratio ( $\text{mgOC m}^{-2}$ ) in sediment cores collected in the West  
 248 Gironde Mud Patch. The yellow stripes indicate the position of noticeable sandy layers. Dashed lines represent the limit  
 249 between modern and relic deposits.

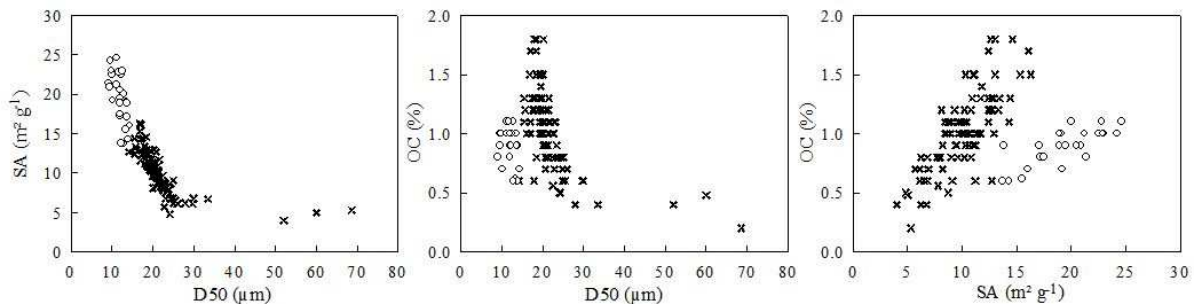
250 A classical way to minimize OC content variations strictly related to grain-size changes is to  
 251 normalized OC values to particle SA (Aller and Blair, 2006; Mayer, 1994a, 1994b). An  
 252 increase of OC/SA ratios in surface sediments is still observed seaward (**Figure 4, Table 2**).  
 253 The profiles of OC/SA ratio show the highest values on cores top followed by a decrease with

254 depth until reaching a quite constant value at cores bottom. Interestingly, a sharp change of  
 255 the OC/SA ratio is observed on profiles of stations 1, 6 and 9 under which they are quite  
 256 constant (**Figure 4**), suggesting the presence of two distinct vertical horizons in the sediment  
 257 columns. These deposits stand out from most sediments of the WGMP by a lower median  
 258 grain-size and a higher SA (**Figure 5**). Besides, we observed during slicing that these  
 259 sediments were visually different, i.e. darker and much stickier. These changes can be related  
 260 to a variation of sediments in term of sources or ages. From these observations, we interpret  
 261 the sedimentary columns of cores 1, 6 and 9 as (1) a top part where modern deposition occurs  
 262 and (2) a bottom part corresponding to old sediments (**Figure 4**). In the rest of the text, the  
 263 two parts of these cores are respectively qualified as “modern” and “relic” deposits.

264 **Table 2:** Surface and bottom core OC contents (%) and OC/SA ratio ( $\text{mgOC m}^{-2}$ ). \*For stations 1, 6 and 9 the bottom values  
 265 were taken at the base of modern sediments.

Stations (Depth)	OC content (%)		OC/SA ( $\text{mgOC m}^{-2}$ )	
	Surface	Bottom	Surface	Bottom
1 (35m)	0.48	0.64*	0.97	0.57*
North 2 (47m)	0.70	0.56	1.14	0.71
3 (55m)	1.15	1.02	1.42	0.96
8 (62m)	1.08	1.01	1.43	1.04
4 (69m)	1.53	1.25	1.49	0.98
6 (37m)	0.36	0.61*	0.89	0.48*
South 7 (50m)	1.09	1.32	1.12	0.98
9 (54m)	0.84	1.25*	1.34	1.07*

266  
 267 The OC/SA ratios at the base of modern sediments vary by more than twice depending on  
 268 stations and increase with bathymetry with values of  $0.5\text{-}0.6 \text{ mgOC m}^{-2}$  at stations 1 and 6,  
 269  $0.6\text{-}0.9 \text{ mgOC m}^{-2}$  at station 2, and about  $1.0 \text{ mgOC m}^{-2}$  at the other (**Figure 4, Table 2**).  
 270 Relic sediments at stations 1, 6 and 9 show quite similar OC/SA ratios of  $0.42 \pm 0.04$ ,  $0.47 \pm$   
 271  $0.04$  and  $0.53 \pm 0.09 \text{ mgOC m}^{-2}$ , respectively (**Figure 4**).



272

273 **Figure 5:** SA against median grain-size (a); Sediment OC content against median grain-size (b) and SA (c). Cross correspond  
 274 to all the sediment samples, excluding the relic sediments (white circles; stations 1, 6 and 9).

#### 275 4. Discussion

276 The sedimentary functioning of the WGMP was first investigated in the late 80s but its  
 277 capability to store organic carbon on a multi-decennial scale remains still unknown. A  
 278 prerequisite of establishing estimates of organic carbon burial rates and efficiencies was then  
 279 to update the present-day sedimentation rates of the area. The potential factors controlling the  
 280 spatial changes of OC burial rates and storage efficiencies are then discussed, and the  
 281 capability of the WGMP to store OC is compared to other continental shelves.

##### 282 4.1 Sedimentation in the WGMP

283 Sedimentary structures and sedimentation rates in the WGMP suggest a zonation of  
 284 sedimentary processes in several areas, which differ by hydrodynamic intensity and the  
 285 constant or transient nature of deposits. The sedimentation appears to be episodic at stations 1,  
 286 6, 7 and 9i. In addition, stations 7 and 9i are characterized by massive but sporadic deposits.  
 287 The sedimentary sequences of interstratified sand and silt layers observed at the most  
 288 proximal stations 1 and 6 are hypothesized to be the result of alternations of fine particles  
 289 inputs during river floods and of sand inputs from the adjacent continental shelf during storms  
 290 (Jouanneau et al., 1989; Lesueur et al., 2002; Weber et al., 1991). The modern sedimentation  
 291 in the proximal area is related to the surface sandy layers, silty deposits being merely seasonal  
 292 and resuspended during high hydrodynamic events (Jouanneau et al., 1989; Lesueur et al.,  
 293 2001), resulting in the lowest SAR reported for the WGMP (**Table 1**). According to literature,  
 294 relic deposits observed at these sites were dated from 3000 (Jouanneau et al., 1989) to few  
 295 hundred years B.P. (Lesueur et al., 2002). The deeper and central areas are likely less  
 296 subjected to hydrodynamic forces (i.e., waves and currents) and thus have higher SAR and  
 297 MAR (**Figure 6, Table 1**).  $^{210}\text{Pb}_{\text{xs}}$  profiles highlight a rather continuous fine sedimentation on  
 298 the deepest stations of the northern (i.e., 3, 8 and 4) and southern (i.e., 9) transects. SAR of  
 299 these sites lie a maximum of  $0.47 \pm 0.05 \text{ cm yr}^{-1}$  on the outer-central part of the area,  
 300 suggesting the presence of a depocenter (**Figure 6, Table 1**). The station 2 seems to  
 301 correspond to a transition area between the proximal and the distal part of the mud patch. It is  
 302 defined by a rather constant sedimentation interspersed by episodic sandy inputs. Besides the  
 303 difference in laminae preservation among sites indicates a variation of sediment dynamic.  
 304 Indeed, the laminae preservation at stations 1, 6 and 7 suggests a high frequency of  
 305 resuspension/deposition events that prevent to observe biological reworking whereas

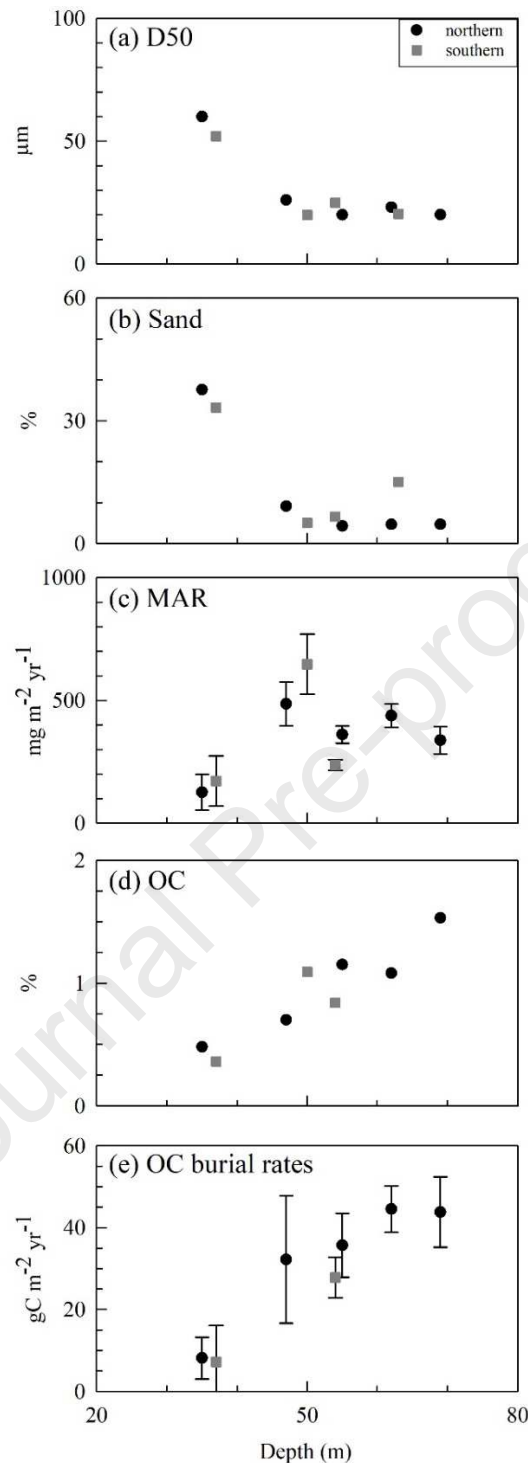
306 completely bioturbated facies are observed at distal sites (i.e., 8 and 4). From these results, the  
307 WGMP can be divided in three sedimentary areas which can be depicted as: (1) a proximal  
308 area subjected to a high hydrodynamics with a low sediment deposition, (2) an outer-central  
309 part with a rather constant sedimentation, and (3) patches where deposits seem massive but  
310 sporadic.

#### 311 *4.2 Quantitative assessment of OC burial rates in the WGMP*

312 Sedimentation intensity and sediment OC content are known to influence OC storage in  
313 sediments (Middelburg, 2019). Therefore, the zonation of sedimentary processes in the  
314 WGMP as well as the offshore increase of surface OC content (**Figure 6, Table 2**) suggest  
315 that organic carbon burial rates vary depending on areas.

316 Mean organic carbon burial rates (BR) were determined by multiplying the sediment mass  
317 accumulation rate by the mean sediment OC content at the base of modern deposits (Berner,  
318 1982; Masqué et al., 2002; Mayer, 1994a). The non-steady state of sedimentary processes at  
319 stations 7 and 9i, precluded the calculation of OC burial rates at these sites. For stations 1 and  
320 6 where the finest fraction is likely to be resuspended during energetic events, burial rates  
321 values must be considered as maximum values for the last decades.

322 On the northern transect, OC burial rates increase seaward from  $8 \pm 5 \text{ gC m}^{-2} \text{ yr}^{-1}$  at station 1  
323 to almost constant values of about  $44 - 45 \text{ gC m}^{-2} \text{ yr}^{-1}$  at depths deeper than 60 m (**Table 2,**  
324 **Figure 6**). Indeed, despite the highest sediment OC contents at station 4, OC burial rates are  
325 equivalent at stations 4 and 8 owing to a higher MAR at station 8 (**Table 2, Figure 6**). This  
326 underlines that sediment accumulation intensity is a major controlling factor of organic  
327 carbon sequestration on a multi-decennial scale as already reported for other systems like the  
328 Rhône delta (Blair and Aller, 2012; Pastor et al., 2011), the Ganges-Brahmaputra Fan (Blair  
329 and Aller, 2012), the Eel shelf (Leithold et al., 2005) and more widely for well-oxygenated  
330 marine sediments (Blair and Aller, 2012; Canfield, 1994). However, the fact that



331

332 **Figure 6:** Median grain-size (a), sand (b) and organic carbon (d) content of surface sediments, mass accumulation rates (c)  
 333 and OC burial rates at multi-decennial scales (e) against water depth of stations along the northern and the southern transects  
 334 of the West Gironde Mud Patch.

335 OC burial rates are lower at station 2 in spite of an important MAR indicates that burial rates  
 336 also depend on OC content. It is indeed lower at this station (**Table 2**) due to the presence of  
 337 coarser sediments. Organic carbon content at the base of modern deposits is related to (1)  
 338 organic carbon inputs which are controlled by the type of sedimentation (sand versus mud)

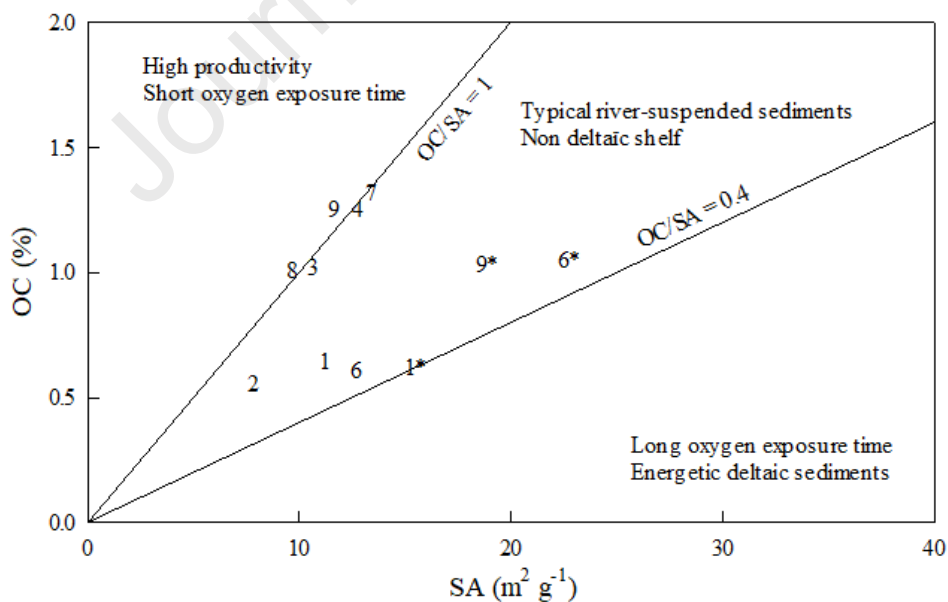


339 and to (2) the extent of organic matter degradation (Middelburg, 2019) whose quantification  
340 is out the scope of this work. There are three sediment sources to the WGMP: (1) the Gironde  
341 estuary whose particles settle mainly in the central and distal areas, (2) a biogenic production  
342 in the water column, and (3) the adjacent continental shelf which supplies sand during  
343 energetic events (Jouanneau et al., 1989; Lesueur et al., 2002; Weber et al., 1991). On the  
344 northern transect, the decrease of surface median grain-size and sand content seaward  
345 indicates a decrease of hydrodynamic intensity with depth (**Figure 6**). This suggests that the  
346 type of sedimentation, and so organic matter inputs, are controlled by the hydrodynamic  
347 intensity. Sand inputs which occur mainly in the proximal area dilute the sedimentary organic  
348 matter whereas higher OC contents are observed in the distal area where hydrodynamic  
349 intensity is lower. This clearly shows that the amount of OC stored in the WGMP is  
350 influenced by both the amount of sedimentary inputs and hydrodynamic intensity.

#### 351 *4.3 Qualitative comparison of OC burial efficiency: direct use of OC content and SA*

352 The OC burial efficiency is typically assessed with the ratio of OC burial rates to inputs  
353 (Burdige, 2007). As these inputs were not quantified in this work, this quantitative approach is  
354 ruled out. Nevertheless, the OC/SA ratio allows a qualitative assessment of organic carbon  
355 burial efficiencies. Blair and Aller (2012) reported that this ratio can be used to define  
356 different types of sedimentary environments (**Figure 7**). Briefly areas with enhanced organic  
357 matter degradation because of frequent sediment remobilization or low sedimentation rates  
358 allowing a long oxygen exposure time are characterized by an OC/SA ratio  $< 0.4 \text{ mgOC m}^{-2}$ .  
359 On the opposite, an OC/SA  $> 1.0 \text{ mgOC m}^{-2}$  reflects an environment with OC inputs higher  
360 than loss through degradation (e.g. upwelling or low-oxygen areas). Intermediate values  
361 between 0.4 and  $1.0 \text{ mgOC m}^{-2}$  are observed on river-suspended particles and non-deltaic  
362 shelf. In the West Gironde Mud Patch, values of OC/SA ratios at the base of modern  
363 sediments are typical of non-deltaic continental shelves (**Table 2, Figure 7**), namely those  
364 which do not receive high sedimentary inputs (Blair and Aller, 2012; Mayer, 1994a). These  
365 values indicate stable organic-mineral associations which protect organic matter from  
366 microbial decomposition and result in a lower organic matter reactivity and availability for  
367 degradation (Blair and Aller, 2012). This can be due to the supply of relatively refractory  
368 organic matter from the Gironde (Etcheber et al., 2007) or to the degradation of organic  
369 matter in the sediments of the WGMP until reaching an OC/SA value from which the organic  
370 carbon is less bioavailable. The increase seaward of OC/SA ratios at the base of modern  
371 sediments indicates an increase of OC storage efficiency (**Table 2, Figure 7**). This is

372 consistent with the decrease of hydrodynamic intensity which controls the extent of sediment  
 373 resuspension. The higher hydrodynamic intensity at proximal sites (i.e., 1 and 6) promotes  
 374 thus sediment organic matter degradation (Aller, 1998; Aller and Blair, 2006; Yao et al.,  
 375 2014) and results in a low OC storage efficiency (**Table 2, Figure 7**). Conversely, OC storage  
 376 efficiencies are the highest in the central and distal WGMP. Interestingly, in spite of higher  
 377 OC burial rates at stations 8 and 4 than at station 3, the three sites seem to be equally efficient  
 378 to store OC (**Figure 7**). Since the OC contents in surface sediments are higher at station 4, this  
 379 suggests that organic matter degradation is more efficient at this station than at station 3. The  
 380 discrepancy between OC burial rates and efficiencies indicates that factors controlling the  
 381 amount of organic carbon stored in sediments are different than those controlling the  
 382 preservation efficiency. Therefore, if hydrodynamic intensity and the amount of sedimentary  
 383 inputs control the quantity of sequestered OC, the intensity of organic matter degradation  
 384 may at least in part influence its storage efficiency. Regarding its efficiency to store OC,  
 385 station 2 can merely be considered as “intermediate”. The OC storage at station 7 appears as  
 386 efficient as at the distal sites (**Figure 7**). This is likely due to the massive sedimentation  
 387 occurring at this station which limits the degradation of organic matter. However, these  
 388 deposits may be only transients. Accordingly, it is quite difficult to clearly determine from  
 389 this study if this storage is efficient on a multi-decennial scale.



390

391 **Figure 7:** Relationship of OC contents (%) against surface areas of sediments (SA;  $\text{m}^2 \text{g}^{-1}$ ) at the base of modern and relic  
 392 (\*) sediments of the West Gironde Mud Patch. Adapted from Blair and Aller (2012).

393 Relic deposits at stations 1 and 9 present lower OC/SA ratios than modern ones (**Figures 4**  
 394 and **7**). A first explanation is to consider a longer degradation duration. However, ratios of

395 modern and relic deposits are equivalents at station 6. Low and constant OC/SA ratios  
396 (**Figure 4**) indicate that organic matter has been extensively degraded and reached an OC  
397 refractory background (Mayer, 1994b, 1994a). This important degradation observed at  
398 stations 1 and 6 is likely related to both degradation duration of organic matter and intense  
399 hydrodynamics in the inner WGMP.

400 The use of OC/SA ratios confirms a zonation of sedimentary processes in the WGMP as  
401 previously argued on the base of sedimentation characteristics (description, intensity). This  
402 could be described in terms of organic carbon storage as: (1) a proximal part characterized by  
403 a decimeter-thick modern layer with a relatively low OC storage efficiency overlying relic  
404 deposits, (2) a distal area which appears as the only efficient zone for OC storage on a multi-  
405 decennial scale, and (3) patches represented by station 7 where apparent efficient OC storage  
406 is likely related to massive sedimentation events. These qualitative estimates of OC burial  
407 efficiencies confirm that the OC sequestration in the WGMP depends in part on the  
408 hydrodynamic intensity which controls sedimentation and resuspension processes. However,  
409 other factors like the intensity of organic matter degradation seem influence OC storage  
410 efficiency in the central and distal WGMP.

#### 411 *4.4 Comparison with other continental shelves*

412 On the Northeast Atlantic margin, numerous sedimentological and biogeochemical studies  
413 have been conducted (Anschutz and Chaillou, 2009; Charbonnier et al., 2019; Herman et al.,  
414 2001; Jouanneau et al., 2002; Mouret et al., 2010; Schmidt et al., 2009; van Weering et al.,  
415 2002, 1998) but only few of them have focused on the OC sequestration in sediments (Epping  
416 et al., 2002; Mouret et al., 2010; van Weering et al., 2002, 1998). Studies conducted on other  
417 areas of the Bay of Biscay margin (Mouret et al., 2010) and on the Celtic (van Weering et al.,  
418 1998) and Iberian margins (van Weering et al., 2002), allow a comparison with organic  
419 carbon burial rates obtained in the WGMP (this work) (**Table 3**). There is a wide range of OC  
420 burial rates from  $<0.5 \text{ gC m}^{-2} \text{ yr}^{-1}$  on the Celtic margin (van Weering et al., 1998) to  $34.3 \text{ gC}$   
421  $\text{m}^{-2} \text{ yr}^{-1}$  on the Iberian shelf (van Weering et al., 2002). Locally, on the Bay of Biscay margin,  
422 organic carbon burial rates decrease with increasing depth, with the highest values observed  
423 for the WGMP (**Table 3**). These high OC burial rates are most likely due to the proximity of  
424 its main sediment source (i.e., the Gironde). Deeper on the slope, the lower organic carbon  
425 burial rates are associated with lower sedimentation rates (**Table 3**, Mouret et al., 2010).  
426 Besides, studies carried out on the Iberian shelf and the Celtic margin (i.e., Epping et al.,  
427 2002; van Weering et al., 2002, 1998) concluded that, as for the WGMP, variations of OC

428 burial rates are related to variations of sedimentation intensity. These comparisons highlight  
 429 that the WGMP is an area of the Northeast Atlantic margin which stores relatively high  
 430 amount of organic carbon on a multi-decennial scale.

431 At a global oceanic scale, Blair and Aller (2012) reported and compared organic carbon burial  
 432 efficiencies of many RiOMars. However quantitative estimates of OC burial rates on  
 433 continental shelves, where fine sedimentation occurs, are mainly related to systems under the  
 434 influence of large rivers, with average values from  $15.3 \text{ gC m}^{-2} \text{ yr}^{-1}$  in the Bohai and Yellow  
 435 Seas (Hu et al., 2016) to  $58.3 \text{ gC m}^{-2} \text{ yr}^{-1}$  in the Amazon deltaic shelf (Aller et al., 1996)  
 436 (**Table 3**). In addition, the spatial extent of these RiOMars (i.e., at least several thousand  
 437 square kilometers) makes them important areas for organic carbon storage (Aller et al., 1996;  
 438 Gordon et al., 2001; Hu et al., 2016; Qiao et al., 2017; Sun et al., 2020). Although the WGMP  
 439 is one with the highest OC burial rates among the Northeast Atlantic margin systems, it  
 440 cannot be considered as a major sink of organic carbon on a global oceanic scale due to its  
 441 small spatial extent (i.e.,  $420 \text{ km}^2$ ).

442 **Table 3:** Mass accumulation rates and OC burial rates in sediments of (1) the West Gironde Mud Patch (this study) (2) the  
 443 Bay of Biscay (Mouret et al., 2010), (3) the Goban Spur (Celtic margin, Van Weering et al., 1998), (4) the Iberian Margin  
 444 (Van Weering et al., 2002), (5) the Gulf of Lions shelf (Accornero et al., 2003) and of (6) the Amazon deltaic shelf (Aller et  
 445 al., 1996; Kuehl et al., 1986), the Bohai and Yellow Seas (Hu et al., 2016), the Zhejiang-Fujian Mud Zone (East China Sea,  
 446 Sun et al., 2020), the inner Louisiana shelf (Gordon et al., 2001). The most proximal sites of the WGMP (i.e., 1 and 6) are not  
 447 considered. \*Average values of organic carbon burial rates.

Location	Depth (m)	MAR ( $\text{mg cm}^{-2} \text{ yr}^{-1}$ )	OC burial rates ( $\text{gC m}^{-2} \text{ yr}^{-1}$ )	References
WGMP (Bay of Biscay)	47 - 69	237 - 486	28 - 45	This study
Bay of Biscay	550	78	7.32	
Bay of Biscay	1000	36	2.52	
Bay of Biscay	1250	44	2.4	Mouret et al. (2010)
Bay of Biscay	1500	7	0.45	
Bay of Biscay	2000	14	0.96	
Goban Spur	208	<5.8	> 0.16	Van Weering et al. (1998)
Iberian Margin	104	204.2	34.30	
Iberian Margin	123	208.9	9.00	
Iberian Margin	199	150.1	7.09	Van Weering et al. (2002)
Iberian Margin	223	157.1	5.02	
Iberian Margin	343	63.4	3.77	
Gulf of Lions	87	230	19.0	Accornero et al. (2003)
Amazon deltaic shelf	9 - 53	100 - 6900	58.3*	Aller et al. (1996), Kuehl et al. (1986)
Bohai and Yellow Seas	0 - 400	< 100 - 7000	15.3*	Hu et al. (2016)

East China Sea	45.4	200 - 700	41.2*	Sun et al. (2020)
Louisiana shelf	4 - 23	120 - 450	22.7*	Gordon et al. (2001)

## 448 **Conclusion**

449 This study aimed to assess a first estimate of organic carbon sequestration in the West  
 450 Gironde Mud Patch sediments. The amount of stored OC increases seaward with a maximum  
 451 value of  $45 \text{ gC m}^{-2} \text{ yr}^{-1}$ . Beyond the quantification, sedimentary structures and  $^{210}\text{Pb}_{\text{xs}}$  profiles  
 452 as well as a qualitative comparison of the capability of each site to store OC allow to divide  
 453 the WGMP in several sedimentary sub-environments: (1) a proximal area where modern  
 454 deposits are a decimeter-thick layer with a relatively low OC storage efficiency, (2) a distal  
 455 part with a relatively efficient OC storage and (3) patches where OC storage seems efficient,  
 456 at least temporarily.

457 The amount of OC sequestered in sediments on a multi-decennial scale is mainly related to  
 458 the amount of sedimentary inputs and to hydrodynamic conditions which controls  
 459 sedimentation intensity and nature (i.e., mud versus sand inputs). However other factors like  
 460 the intensity of organic matter degradation seem to influence the efficiency of OC  
 461 preservation in sediments in the central and distal areas. Further studies are therefore need to  
 462 define and quantify processes which can influence this preservation in the West Gironde Mud  
 463 Patch on a multi-decennial scale but also on other time scales (seasonal, inter-annual, multi-  
 464 secular). At the scale of the Northeast Atlantic margin, the West Gironde Mud Patch appears  
 465 efficient in storing organic carbon but its contribution to the OC storage at larger scale  
 466 remains quite low because of its small surface area. Nevertheless, considering all mud patches  
 467 of the Bay of Biscay continental shelf (e.g., La Grande Vasière, the Basque Mud Patch), the  
 468 OC storage can be potentially significant at the North-Atlantic scale. Accordingly, it appears  
 469 necessary to led further studies on these areas to define their capabilities to store organic  
 470 carbon.

## 471 **Acknowledgements**

472 We sincerely acknowledge the captains and crews of the R/V “Côtes de la Manche” (CNRS-  
 473 INSU) for their great help during the JERICOBENT-1 cruise. We also thank Rémy Synais for  
 474 his work on sampling and analyses as well as François Dano for the preparation of an updated  
 475 map of the WGMP during his Master 2 dissertation. This work was supported by: (1) the  
 476 JERICO-NEXT project (European Union's Horizon 2020 Research and Innovation program  
 477 under grant agreement no. 654410), (2) the VOG project (national program Interface LEFE-  
 478 EC2CO). The cruise was funded by the French Oceanographic Fleet (DOI:

479 10.17600/16010400). A doctoral fellowship was provided to N. Dubosq by the french  
 480 Ministry of Higher Education, Research and Innovation. We are thankful to the French  
 481 Nouvelle Aquitaine Research Council (E3A Project) for co-funding both the low-  
 482 background gamma detector and the microelectrode system equipped with a camera. We also  
 483 thank the UMR 5805 EPOC for co-funding the Surface Area Analyzer.

#### 484 **References**

- 485 Accornero, A., Picon, P., Bovée, F. de, Charrière, B., Buscail, R., 2003. Organic carbon  
 486 budget at the sediment–water interface on the Gulf of Lions continental margin.  
 487 *Continental Shelf Research* 23, 79–92. [https://doi.org/10.1016/S0278-4343\(02\)00168-](https://doi.org/10.1016/S0278-4343(02)00168-1)  
 488 1
- 489 Allen, G.P., Castaing, P., 1977. Carte de répartition des sédiments superficiels sur le plateau  
 490 continental du Golfe de Gascogne. *Bulletin Institut de Géologie du Bassin d’Aquitaine*  
 491 (Bordeaux) 255–261.
- 492 Aller, R.C., 1998. Mobile deltaic and continental shelf muds as suboxic, fluidized bed  
 493 reactors. *Marine Chemistry* 61, 143–155. [https://doi.org/10.1016/S0304-](https://doi.org/10.1016/S0304-4203(98)00024-3)  
 494 4203(98)00024-3
- 495 Aller, R.C., Blair, N.E., 2006. Carbon remineralization in the Amazon–Guianas tropical  
 496 mobile mudbelt: A sedimentary incinerator. *Continental Shelf Research, Special Issue*  
 497 *in Honor of Richard W. Sternberg’s Contributions to Marine Sedimentology* 26,  
 498 2241–2259. <https://doi.org/10.1016/j.csr.2006.07.016>
- 499 Aller, R.C., Blair, N.E., Xia, Q., Rude, P.D., 1996. Remineralization rates, recycling, and  
 500 storage of carbon in Amazon shelf sediments. *Continental Shelf Research* 16, 753–  
 501 786. [https://doi.org/10.1016/0278-4343\(95\)00046-1](https://doi.org/10.1016/0278-4343(95)00046-1)
- 502 Aller, R.C., Mackin, J.E., Cox, R.T., 1986. Diagenesis of Fe and S in Amazon inner shelf  
 503 muds: apparent dominance of Fe reduction and implications for the genesis of  
 504 ironstones. *Continental Shelf Research* 6, 263–289. [https://doi.org/10.1016/0278-](https://doi.org/10.1016/0278-4343(86)90064-6)  
 505 4343(86)90064-6
- 506 Anschutz, P., Chaillou, G., 2009. Deposition and fate of reactive Fe, Mn, P, and C in  
 507 suspended particulate matter in the Bay of Biscay. *Continental Shelf Research* 29,  
 508 1038–1043. <https://doi.org/10.1016/j.csr.2008.12.022>
- 509 Berner, R.A., 1990. Atmospheric Carbon Dioxide Levels Over Phanerozoic Time. *Science*  
 510 249, 1382–1386. <https://doi.org/10.1126/science.249.4975.1382>
- 511 Berner, R.A., 1982. Burial of organic carbon and pyrite sulfur in the modern ocean; its  
 512 geochemical and environmental significance. *American Journal of Science* 282, 451–  
 513 473. <https://doi.org/10.2475/ajs.282.4.451>
- 514 Blair, N.E., Aller, R.C., 2012. The Fate of Terrestrial Organic Carbon in the Marine  
 515 Environment. *Annual Review of Marine Science* 4, 401–423.  
 516 <https://doi.org/10.1146/annurev-marine-120709-142717>
- 517 Borja, A., Amouroux, D., Anschutz, P., Gómez-Gesteira, M., Uyarra, M.C., Valdés, L., 2019.  
 518 The Bay of Biscay, in: *World Seas: An Environmental Evaluation*. Elsevier, pp. 113–  
 519 152. <https://doi.org/10.1016/B978-0-12-805068-2.00006-1>
- 520 Bourillet, J.-F., Zaragosi, S., Mulder, T., 2006. The French Atlantic margin and deep-sea  
 521 submarine systems. *Geo-Marine Letters* 26, 311–315. [https://doi.org/10.1007/s00367-](https://doi.org/10.1007/s00367-006-0042-2)  
 522 006-0042-2

- 523 Burdige, D.J., 2007. Preservation of Organic Matter in Marine Sediments: Controls,  
 524 Mechanisms, and an Imbalance in Sediment Organic Carbon Budgets? *Chemical*  
 525 *Reviews* 107, 467–485. <https://doi.org/10.1021/cr050347q>
- 526 Canfield, D.E., 1994. Factors influencing organic carbon preservation in marine sediments.  
 527 *Chemical Geology* 114, 315–329. [https://doi.org/10.1016/0009-2541\(94\)90061-2](https://doi.org/10.1016/0009-2541(94)90061-2)
- 528 Cauwet, G., Gadel, F., de Souza Sierra, M.M., Donard, O., Ewald, M., 1990. Contribution of  
 529 the Rhône River to organic carbon inputs to the northwestern Mediterranean Sea.  
 530 *Continental Shelf Research* 10, 1025–1037. [https://doi.org/10.1016/0278-](https://doi.org/10.1016/0278-4343(90)90073-U)  
 531 [4343\(90\)90073-U](https://doi.org/10.1016/0278-4343(90)90073-U)
- 532 Charbonnier, C., Mouret, A., Howa, H., Schmidt, S., Gillet, H., Anschutz, P., 2019.  
 533 Quantification of diagenetic transformation of continental margin sediments at the  
 534 Holocene time scale. *Continental Shelf Research* 180, 63–74.  
 535 <https://doi.org/10.1016/j.csr.2019.04.015>
- 536 Constantin, S., Doxaran, D., Derkacheva, A., Novoa, S., Lavigne, H., 2018. Multi-temporal  
 537 dynamics of suspended particulate matter in a macro-tidal river Plume (the Gironde)  
 538 as observed by satellite data. *Estuarine, Coastal and Shelf Science* 202, 172–184.  
 539 <https://doi.org/10.1016/j.ecss.2018.01.004>
- 540 Deflandre B., 2016. JERICOBENT-1 cruise, Côtes De La Manche R/V.  
 541 <https://doi.org/10.17600/16010400>
- 542 Deng, B., Zhang, J., Wu, Y., 2006. Recent sediment accumulation and carbon burial in the  
 543 East China Sea. *Global Biogeochemical Cycles* 20.  
 544 <https://doi.org/10.1029/2005GB002559>
- 545 Dias, J.M.A., Jouanneau, J.M., Gonzalez, R., Araújo, M.F., Drago, T., Garcia, C., Oliveira,  
 546 A., Rodrigues, A., Vitorino, J., Weber, O., 2002. Present day sedimentary processes  
 547 on the northern Iberian shelf. *Progress in Oceanography, Benthic processes and*  
 548 *dynamics at the NW Iberian Margin: results of the OMEX II Program* 52, 249–259.  
 549 [https://doi.org/10.1016/S0079-6611\(02\)00009-5](https://doi.org/10.1016/S0079-6611(02)00009-5)
- 550 Epping, E., van der Zee, C., Soetaert, K., Helder, W., 2002. On the oxidation and burial of  
 551 organic carbon in sediments of the Iberian margin and Nazaré Canyon (NE Atlantic).  
 552 *Progress in Oceanography* 52, 399–431. [https://doi.org/10.1016/S0079-](https://doi.org/10.1016/S0079-6611(02)00017-4)  
 553 [6611\(02\)00017-4](https://doi.org/10.1016/S0079-6611(02)00017-4)
- 554 Etcheber, H., Relexans, J.-C., Beliard, M., Weber, O., Buscail, R., Heussner, S., 1999.  
 555 Distribution and quality of sedimentary organic matter on the Aquitanian margin (Bay  
 556 of Biscay). *Deep Sea Research Part II: Topical Studies in Oceanography* 46, 2249–  
 557 2288. [https://doi.org/10.1016/S0967-0645\(99\)00062-4](https://doi.org/10.1016/S0967-0645(99)00062-4)
- 558 Etcheber, H., Taillez, A., Abril, G., Garnier, J., Servais, P., Moatar, F., Commarieu, M.-V.,  
 559 2007. Particulate organic carbon in the estuarine turbidity maxima of the Gironde,  
 560 Loire and Seine estuaries: origin and lability. *Hydrobiologia* 588, 245–259.  
 561 <https://doi.org/10.1007/s10750-007-0667-9>
- 562 Gillet, H., Deflandre, B., 2018. JERICOBENT-5-TH cruise, Thalia R/V.  
 563 <https://doi.org/10.17600/18000425>
- 564 Gordon, E.S., Goñi, M.A., Roberts, Q.N., Kineke, G.C., Allison, M.A., 2001. Organic matter  
 565 distribution and accumulation on the inner Louisiana shelf west of the Atchafalaya  
 566 River. *Continental Shelf Research* 21, 1691–1721. [https://doi.org/10.1016/S0278-](https://doi.org/10.1016/S0278-4343(01)00021-8)  
 567 [4343\(01\)00021-8](https://doi.org/10.1016/S0278-4343(01)00021-8)
- 568 Hedges, J.I., Keil, R.G., 1995. Sedimentary organic matter preservation: an assessment and  
 569 speculative synthesis. *Marine Chemistry* 49, 81–115. [https://doi.org/10.1016/0304-](https://doi.org/10.1016/0304-4203(95)00008-F)  
 570 [4203\(95\)00008-F](https://doi.org/10.1016/0304-4203(95)00008-F)
- 571 Herman, P.M.J., Soetaert, K., Middelburg, J.J., Heip, C., Lohse, L., Epping, E., Helder, W.,  
 572 Antia, A.N., Peinert, R., 2001. The seafloor as the ultimate sediment trap—using

- 573 sediment properties to constrain benthic–pelagic exchange processes at the Goban  
 574 Spur. *Deep Sea Research Part II: Topical Studies in Oceanography* 48, 3245–3264.  
 575 [https://doi.org/10.1016/S0967-0645\(01\)00039-X](https://doi.org/10.1016/S0967-0645(01)00039-X)
- 576 Hu, L., Shi, X., Bai, Y., Qiao, S., Li, L., Yu, Y., Yang, G., Ma, D., Guo, Z., 2016. Recent  
 577 organic carbon sequestration in the shelf sediments of the Bohai Sea and Yellow Sea,  
 578 China. *Journal of Marine Systems* 155, 50–58.  
 579 <https://doi.org/10.1016/j.jmarsys.2015.10.018>
- 580 Jouanneau, J.-M., Weber, O., Champilou, N., Cirac, P., Muxika, I., Borja, A., Pascual, A.,  
 581 Rodríguez-Lázaro, J., Donard, O., 2008. Recent sedimentary study of the shelf of the  
 582 Basque country. *Journal of Marine Systems, Oceanography of the Bay of Biscay* 72,  
 583 397–406. <https://doi.org/10.1016/j.jmarsys.2007.03.013>
- 584 Jouanneau, J.M., Weber, O., Cremer, M., Castaing, P., 1999. Fine-grained sediment budget on  
 585 the continental margin of the Bay of Biscay. *Deep Sea Research Part II: Topical  
 586 Studies in Oceanography* 46, 2205–2220. [https://doi.org/10.1016/S0967-  
 587 0645\(99\)00060-0](https://doi.org/10.1016/S0967-0645(99)00060-0)
- 588 Jouanneau, J.M., Weber, O., Drago, T., Rodrigues, A., Oliveira, A., Dias, J.M.A., Garcia, C.,  
 589 Schmidt, S., Reyss, J.L., 2002. Recent sedimentation and sedimentary budgets on the  
 590 western Iberian shelf. *Progress in Oceanography, Benthic processes and dynamics at  
 591 the NW Iberian Margin: results of the OMEX II Program* 52, 261–275.  
 592 [https://doi.org/10.1016/S0079-6611\(02\)00010-1](https://doi.org/10.1016/S0079-6611(02)00010-1)
- 593 Jouanneau, J.M., Weber, O., Latouche, C., Vernet, J.P., Dominik, J., 1989. Erosion, non-  
 594 deposition and sedimentary processes through a sedimentological and radioisotopic  
 595 study of surficial deposits from the “Ouest-Gironde vasière” (Bay of Biscay).  
 596 *Continental Shelf Research* 9, 325–342. [https://doi.org/10.1016/0278-4343\(89\)90037-  
 597 X](https://doi.org/10.1016/0278-4343(89)90037-X)
- 598 Keil, R., 2017. Anthropogenic Forcing of Carbonate and Organic Carbon Preservation in  
 599 Marine Sediments. *Annual Review of Marine Science* 9, 151–172.  
 600 <https://doi.org/10.1146/annurev-marine-010816-060724>
- 601 Kuehl, S.A., DeMaster, D.J., Nittrouer, C.A., 1986. Nature of sediment accumulation on the  
 602 Amazon continental shelf. *Continental Shelf Research* 6, 209–225.  
 603 [https://doi.org/10.1016/0278-4343\(86\)90061-0](https://doi.org/10.1016/0278-4343(86)90061-0)
- 604 Kuzyk, Z.Z.A., Gobeil, C., Goñi, M.A., Macdonald, R.W., 2017. Early diagenesis and trace  
 605 element accumulation in North American Arctic margin sediments. *Geochimica et  
 606 Cosmochimica Acta* 203, 175–200. <https://doi.org/10.1016/j.gca.2016.12.015>
- 607 Leithold, E.L., Perkey, D.W., Blair, N.E., Creamer, T.N., 2005. Sedimentation and carbon  
 608 burial on the northern California continental shelf: the signatures of land-use change.  
 609 *Continental Shelf Research* 25, 349–371. <https://doi.org/10.1016/j.csr.2004.09.015>
- 610 Lesueur, P., Jouanneau, J.-M., Boust, D., Tastet, J.-P., Weber, O., 2001. Sedimentation rates  
 611 and fluxes in the continental shelf mud fields in the Bay of Biscay (France).  
 612 *Continental Shelf Research* 21, 1383–1401. [https://doi.org/10.1016/S0278-  
 613 4343\(01\)00004-8](https://doi.org/10.1016/S0278-4343(01)00004-8)
- 614 Lesueur, P., Tastet, J.P., Marambat, L., 1996. Shelf mud fields formation within historical  
 615 times: examples from offshore the Gironde estuary, France. *Continental Shelf  
 616 Research* 16, 1849–1870. [https://doi.org/10.1016/0278-4343\(96\)00013-1](https://doi.org/10.1016/0278-4343(96)00013-1)
- 617 Lesueur, P., Tastet, J.P., Weber, O., 2002. Origin and morphosedimentary evolution of fine-  
 618 grained modern continental shelf deposits: the Gironde mud fields (Bay of Biscay,  
 619 France). *Sedimentology* 49, 1299–1320. [https://doi.org/10.1046/j.1365-  
 620 3091.2002.00498.x](https://doi.org/10.1046/j.1365-3091.2002.00498.x)



- 621 Lesueur, P., Tastet, J.-P., Weber, O., Sinko, J.-A., 1991. Modèle faciologique d'un corps  
 622 sédimentaire pélagique de plate-forme: la vasière Ouest-Gironde (France).  
 623 *Oceanologica Acta* sp., 143–153.
- 624 Lofi, J., Werber, O., 2001. SCOPIX - digital processing of X-ray images for the enhancement  
 625 of sedimentary structures in undisturbed core slabs. *Geo-Marine Letters* 20, 182–186.  
 626 <https://doi.org/10.1007/s003670000051>
- 627 Masqué, P., Isla, E., Sanchez-Cabeza, J.A., Palanques, A., Bruach, J.M., Puig, P., Guillén, J.,  
 628 2002. Sediment accumulation rates and carbon fluxes to bottom sediments at the  
 629 Western Bransfield Strait (Antarctica). *Deep Sea Research Part II: Topical Studies in*  
 630 *Oceanography, FRUELA - A Carbon Flux Study in the Antarctic Peninsula Area* 49,  
 631 921–933. [https://doi.org/10.1016/S0967-0645\(01\)00131-X](https://doi.org/10.1016/S0967-0645(01)00131-X)
- 632 Massé, C., Meisterhans, G., Deflandre, B., Bachelet, G., Bourasseau, L., Bichon, S., Ciutat,  
 633 A., Jude-Lemelleur, F., Lavesque, N., Raymond, N., Grémare, A., Garabetian, F.,  
 634 2016. Bacterial and macrofaunal communities in the sediments of the West Gironde  
 635 Mud Patch, Bay of Biscay (France). *Estuarine, Coastal and Shelf Science, Special*  
 636 *Issue: Functioning and dysfunctioning of Marine and Brackish Ecosystems* 179, 189–  
 637 200. <https://doi.org/10.1016/j.ecss.2016.01.011>
- 638 Mayer, L.M., 1994a. Surface area control of organic carbon accumulation in continental shelf  
 639 sediments. *Geochimica et Cosmochimica Acta* 58, 1271–1284.  
 640 [https://doi.org/10.1016/0016-7037\(94\)90381-6](https://doi.org/10.1016/0016-7037(94)90381-6)
- 641 Mayer, L.M., 1994b. Relationships between mineral surfaces and organic carbon  
 642 concentrations in soils and sediments. *Chemical Geology* 114, 347–363.  
 643 [https://doi.org/10.1016/0009-2541\(94\)90063-9](https://doi.org/10.1016/0009-2541(94)90063-9)
- 644 McCave, I.N., 1972. Shelf Sediment Transport, Process and Pattern, in: Swift, D.J.P., Duane,  
 645 D.B., Pilkey, O.H. (Eds.), *Transport and Escape of Fine-Grained Sediment from Shelf*  
 646 *Areas*. Dowden, Hutchinson & Ross, Stroudsburg, Pa., pp. 225–248.
- 647 McKee, B.A., Aller, R.C., Allison, M.A., Bianchi, T.S., Kineke, G.C., 2004. Transport and  
 648 transformation of dissolved and particulate materials on continental margins  
 649 influenced by major rivers: benthic boundary layer and seabed processes. *Continental*  
 650 *Shelf Research* 24, 899–926. <https://doi.org/10.1016/j.csr.2004.02.009>
- 651 Middelburg, J.J., 2019. Carbon Processing at the Seafloor, in: *China's Provincial Economic*  
 652 *Competitiveness and Policy Outlook for the 13th Five-Year Plan Period (2016-2020)*.  
 653 Springer Singapore, Singapore, pp. 57–75. [https://doi.org/10.1007/978-3-030-10822-](https://doi.org/10.1007/978-3-030-10822-9_4)  
 654 [9\\_4](https://doi.org/10.1007/978-3-030-10822-9_4)
- 655 Mouret, A., Anschutz, P., Deflandre, B., Chaillou, G., Hyacinthe, C., Deborde, J., Etcheber,  
 656 H., Jouanneau, J.-M., Grémare, A., Lecroart, P., 2010. Oxygen and organic carbon  
 657 fluxes in sediments of the Bay of Biscay. *Deep Sea Research Part I: Oceanographic*  
 658 *Research Papers* 57, 528–540. <https://doi.org/10.1016/j.dsr.2009.12.009>
- 659 Muller-Karger, F.E., 2005. The importance of continental margins in the global carbon cycle.  
 660 *Geophysical Research Letters* 32, L01602. <https://doi.org/10.1029/2004GL021346>
- 661 Pastor, L., Cathalot, C., Deflandre, B., Viollier, E., Soetaert, K., Meysman, F.J.R., Ulses, C.,  
 662 Metzger, E., Rabouille, C., 2011. Modeling biogeochemical processes in sediments  
 663 from the Rhône River prodelta area (NW Mediterranean Sea). *Biogeosciences* 8,  
 664 1351–1366. <https://doi.org/10.5194/bg-8-1351-2011>
- 665 Pastor, L., Rabouille, C., Metzger, E., Thibault de Chanvalon, A., Viollier, E., Deflandre, B.,  
 666 2018. Transient early diagenetic processes in Rhône prodelta sediments revealed in  
 667 contrasting flood events. *Continental Shelf Research* 166, 65–76.  
 668 <https://doi.org/10.1016/j.csr.2018.07.005>
- 669 Qiao, S., Shi, X., Wang, G., Zhou, L., Hu, B., Hu, L., Yang, G., Liu, Y., Yao, Z., Liu, S.,  
 670 2017. Sediment accumulation and budget in the Bohai Sea, Yellow Sea and East

- 671 China Sea. Marine Geology 390, 270–281.  
 672 <https://doi.org/10.1016/j.margeo.2017.06.004>
- 673 Relexans, J.-C., Lin, R.G., Castel, J., Etcheber, H., Laborde, P., 1992. Response of biota to  
 674 sedimentary organic matter quality of the West Gironde mud patch, Bay of Biscay  
 675 (France). *Oceanologica Acta* 15, 639–649.
- 676 Schmidt, S., 2020. Depth profiles of selected radionuclides and grain size in marine sediments  
 677 of the West Gironde Mud Patch (Bay of Biscay). <https://doi.org/10.17882/77523>
- 678 Schmidt, S., Howa, H., Diallo, A., Martín, J., Cremer, M., Duros, P., Fontanier, C., Deflandre,  
 679 B., Metzger, E., Mulder, T., 2014. Recent sediment transport and deposition in the  
 680 Cap-Ferret Canyon, South-East margin of Bay of Biscay. *Deep Sea Research Part II:  
 681 Topical Studies in Oceanography* 104, 134–144.  
 682 <https://doi.org/10.1016/j.dsr2.2013.06.004>
- 683 Schmidt, S., Howa, H., Mouret, A., Lombard, F., Anschutz, P., Labeyrie, L., 2009. Particle  
 684 fluxes and recent sediment accumulation on the Aquitanian margin of Bay of Biscay.  
 685 *Continental Shelf Research, 100 Years of Research within the Bay of Biscay* 29,  
 686 1044–1052. <https://doi.org/10.1016/j.csr.2008.11.018>
- 687 Sun, X., Fan, D., Liu, M., Liao, H., Tian, Y., 2020. The fate of organic carbon burial in the  
 688 river-dominated East China Sea: Evidence from sediment geochemical records of the  
 689 last 70 years. *Organic Geochemistry* 143, 103999.  
 690 <https://doi.org/10.1016/j.orggeochem.2020.103999>
- 691 van Weering, T.C.E., de Stigter, H.C., Boer, W., de Haas, H., 2002. Recent sediment transport  
 692 and accumulation on the NW Iberian margin. *Progress in Oceanography, Benthic  
 693 processes and dynamics at the NW Iberian Margin: results of the OMEX II Program*  
 694 52, 349–371. [https://doi.org/10.1016/S0079-6611\(02\)00015-0](https://doi.org/10.1016/S0079-6611(02)00015-0)
- 695 van Weering, Tj.C.E., Hall, I.R., de Stigter, H.C., McCave, I.N., Thomsen, L., 1998. Recent  
 696 sediments, sediment accumulation and carbon burial at Goban Spur, N.W. European  
 697 Continental Margin (47–50°N). *Progress in Oceanography* 42, 5–35.  
 698 [https://doi.org/10.1016/S0079-6611\(98\)00026-3](https://doi.org/10.1016/S0079-6611(98)00026-3)
- 699 Walsh, J.P., Nittrouer, C.A., 2009. Understanding fine-grained river-sediment dispersal on  
 700 continental margins. *Marine Geology* 263, 34–45.  
 701 <https://doi.org/10.1016/j.margeo.2009.03.016>
- 702 Weber, O., Jouanneau, J.M., Ruch, P., Mirmand, M., 1991. Grain-size relationship between  
 703 suspended matter originating in the Gironde estuary and shelf mud-patch deposits.  
 704 *Marine Geology* 96, 159–165. [https://doi.org/10.1016/0025-3227\(91\)90213-N](https://doi.org/10.1016/0025-3227(91)90213-N)
- 705 Włodarska-Kowalczyk, M., Mazurkiewicz, M., Górska, B., Michel, L.N., Jankowska, E.,  
 706 Zaborska, A., 2019. Organic Carbon Origin, Benthic Faunal Consumption, and Burial  
 707 in Sediments of Northern Atlantic and Arctic Fjords (60–81°N). *Journal of  
 708 Geophysical Research: Biogeosciences* 124, 3737–3751.  
 709 <https://doi.org/10.1029/2019JG005140>
- 710 Yao, P., Zhao, B., Bianchi, T.S., Guo, Z., Zhao, M., Li, D., Pan, H., Wang, J., Zhang, T., Yu,  
 711 Z., 2014. Remineralization of sedimentary organic carbon in mud deposits of the  
 712 Changjiang Estuary and adjacent shelf: Implications for carbon preservation and  
 713 authigenic mineral formation. *Continental Shelf Research* 91, 1–11.  
 714 <https://doi.org/10.1016/j.csr.2014.08.010>
- 715 Zhu, C., Wagner, T., Talbot, H.M., Weijers, J.W.H., Pan, J.-M., Pancost, R.D., 2013.  
 716 Mechanistic controls on diverse fates of terrestrial organic components in the East  
 717 China Sea. *Geochimica et Cosmochimica Acta* 117, 129–143.  
 718 <https://doi.org/10.1016/j.gca.2013.04.015>
- 719 Zhu, M.-X., Chen, K.-K., Yang, G.-P., Fan, D.-J., Li, T., 2016. Sulfur and iron diagenesis in  
 720 temperate unsteady sediments of the East China Sea inner shelf and a comparison with

721 tropical mobile mud belts (MMBs): S and Fe Diagenesis in Sediments. Journal of  
722 Geophysical Research: Biogeosciences 121, 2811–2828.  
723 <https://doi.org/10.1002/2016JG003391>  
724

Journal Pre-proof

**Highlights**

- The West Gironde Mud Patch can be divided in three deposition areas
- Organic carbon (OC) burial rates increase seaward with a maximum of  $45 \text{ gC m}^{-2} \text{ yr}^{-1}$
- Hydrodynamic seems to control organic carbon burial at a multi-decennial scale
- OC burial rates and efficiencies vary depending on bathymetry

**Declaration of interests**

The authors declare that they have no known competing financial interests or personal relationships that could have appeared to influence the work reported in this paper.

The authors declare the following financial interests/personal relationships which may be considered as potential competing interests:

Journal Pre-proof